AILERON-FLAP-INTEGRATED ROLL CONTROL LAW BY OPTIMIZED CONTROL ALLOCATION FOR FLEXIBLE TRANSPORT AIRCRAFT

Hannes Wilke[1], Géfferson C. Silva[1] & Flávio J. Silvestre[1]

[1]Fachgebiet für Flugmechanik, Flugreglung & Aeroelastizität, Technische Universität Berlin, 10587 Berlin, Germany

Abstract

This paper is emphasizing the control allocation for the lateral control of a more flexible transport aircraft. In general, modern aircraft are equipped with more control effectors than primary (rigid-body) degrees of freedom. Such over-actuated systems allow to regard additional, secondary requirements when deciding on how each available control surface shall contribute to the desired motion of the aircraft. For this purpose, a novel control allocation method, the so-called extended control allocation, is introduced in this paper. This approach directly incorporates aeroelastic states into the control allocation problem, which shall improve the influence of the flexible dynamics on the path control. This allocation algorithm is then compared with two conventional allocation methods, outlining its benefits for the control allocation design of a more flexible aircraft.

Keywords: control allocation, flight control design, more flexible aircraft, multi-functional control devices

1. Introduction

In the last decades, decreasing the environmental impact of commercial aviation has become one of the most important aims in aircraft design. Two important innovations to accomplish this ambitious goal are, among others, the decrease of the structural weight by using composite materials instead of metal [1] and the improvement of the aerodynamic efficiency by increasing the wing's aspect ratio [2]. Both of these developments lead to more flexible wing structures, bringing new challenges for the design of flight control systems. One general consequence is the reduction of the frequency separation between the structural and rigid-body dynamics, which may cause undesirable but unavoidable couplings [3]. In addition, an increased wing flexibility may amplify the adverse yaw effect and cause a more significant non-minimal phase behavior of the roll motion, which makes the lateral aircraft control especially challenging [4]. Furthermore, the flexibility of the wing reduces the aileron efficiency since its deflection causes a counteracting torsion of the wing itself [5].

For past aircraft generations, the design of flight control systems was done based on rigid-body dynamics with quasi-stationary aeroelastic corrections. The juncture of such rigid-body-based controllers with filtering strategies, e.g. notch filtering, ensured a well-performing flight control system for slightly flexible aircraft but is getting to its limits for modern, more flexible aircraft designs [6]. Therefore, new strategies and approaches to mitigate the influences of increased flexibility on path control performance are necessary. Previous publications on the trajectory control of flexible transport aircraft have emphasized the integration of gust and especially maneuver load alleviation systems to achieve a good trajectory tracking performance and to ensure the structural integrity of the airframe. This can be achieved by various strategies, e.g. aeroelastic feedback [7], morphing wing structures [8] or LIDAR based gust feedforward control [9].

Besides integrating additional functions into the flight control system, the coupling of rigid-body and flexible dynamics can also be reduced by allocating the path control inputs such that their effect on the flexible dynamics is minimized. One example is the Airbus A380, for which the three ailerons per wing are deflected with different time offsets so that the excitation of the wing bending is reduced [10].

Another strategy is to maximize the roll effectiveness of the aileron by properly placing them along the wing span. In a work by Sanghi et al. [11] this is investigated by analyzing the influence of the spanwise aileron position on the roll effectiveness for different levels of wing flexibility. It is concluded that the higher the flexibility, the lower the effectiveness of an aileron placed in the conventional position near the wing tip. This is due to the mentioned counteracting wing torsion, which is more pronounced for a more flexible, i.e. less stiff, wing. Furthermore, with increasing airspeed the most effective aileron position moves towards the wing root [11]. While this effect is also aggravated by increasing wing flexibility, it has already been observed for former generations of aircraft. So far, this is accounted for by adding additional roll control surfaces for high-speed roll control close to the wing root, e.g. so-called flaperons on the Boeing 777 [12], which can be seen in Fig. 1. The disadvantages of such separate control surfaces are, among others, additional weight and additional maintenance costs.

Figure 1 – Boeing 777-300 Flaperon Deflected during Cruise Flight [13]

In modern aircraft design, high-lift devices serve multiple purposes besides providing additional lift and drag during take-off and landing. In the Airbus A350 for example, the flaps are shifted during cruise to alter the wing's camber and thereby reduce drag [14]. Recent research goes even further and considers multi-functional control devices rather than single-purpose control surfaces [15]. In this context, some studies propose continously moving flaps which would inherently require new, faster actuating concepts [16]. It is therefore worth investigating the potential use of flaps for roll control as they are in a favorable position and would make additional control surfaces like flaperons with their mentioned disadvantages obsolete.
In this context, the objective of this paper is to design, implement, and numerically test a control allocation for roll control that uses both aileron and flaps so that the influence of the aircraft's flexibility on the roll performance can be reduced. This concept is refereed to as Extended Inverse Control Allocation (short ECA) as it extends the general problem used for the the pseudo-inverse control allocation. The concept is to directly account for the control surfaces' structure dynamical effects during the allocation design, enabling high roll effectiveness with minimal excitation of the aeroelastic modes. This control allocation is then implemented and tested with a simulation model of the DLR D2AE, a high aspect ratio, single-aisle transport aircraft.

2. Control Allocation

Conventionally, an aircraft is equipped with a pair of ailerons and a rudder to control the lateral dynamics, i.e. the rolling and yawing motion. In this case there are two inputs to control two degrees of freedom, which results in a unique solution for the control problem. As modern aircraft provide multiple, redundant control effectors, e.g. multiple ailerons, there is more than one way to achieve the same lateral aircraft behavior. Such systems are referred to as over-actuated systems, meaning there are more control inputs than degrees of freedom to be controlled, allowing for additional design requirements which are typically achieved by control allocation functions. This section provides a general overview on the theory of control allocation as well as an in-depth analysis of the pseudo-inverse control allocation method, upon which the algorithm presented in this paper is based.

2.1 General Control Allocation Problem

Given a state space model of a dynamic system stated as:

$$\dot{x} = \mathbf{A}x + \mathbf{B}u \tag{1}$$

$$y = \mathbf{C}x + \mathbf{D}u \tag{2}$$

with the dynamic matrix $\mathbf{A} \in \mathbb{R}^{n\times n}$, control matrix $\mathbf{B} \in \mathbb{R}^{n\times m}$, output matrix $\mathbf{C} \in \mathbb{R}^{k\times n}$, feed-through matrix $\mathbf{D} \in \mathbb{R}^{k\times m}$, state vector $x \in \mathbb{R}^n$, control vector $u \in \mathbb{R}^m$ and output vector $y \in \mathbb{R}^k$. The initial system acceleration $\dot{x}_{init}$ based on Eq. 1 can be reordered as:

$$\dot{\vec{x}}_{init} = \dot{x}(x=0) = \mathbf{B}u = \begin{bmatrix} \mathbf{B}_{inner} \\ \mathbf{B}_{remain} \end{bmatrix} u = \begin{bmatrix} \dot{x}_{init,inner} \\ \dot{x}_{init,remain} \end{bmatrix} \tag{3}$$

The inner sub-system $\dot{x}_{init,inner}$ consists of $\tilde{n}$ directly affectable states, which in the context of flight mechanics are typically angular accelerations [17]. Meanwhile, the remaining sub-system $\dot{x}_{init,remain}$ consists of all states not considered in the inner sub-system, e.g. aeroelastic states or indirectly affected rigid-body states such as attitude angles, altitude or airspeed. Accordingly, $\mathbf{B}_{inner}\mathbb{R}^{\tilde{n}\times m}$ consists of the rows of the $\mathbf{B}$ matrix corresponding to the states in $\dot{x}_{init,inner}$ while $\mathbf{B}_{remain}$ consists of the remaining rows. The general objective of a control allocation problem is to coordinate the elements of the control vector u in such a way that the initial response of inner sub-system $\dot{x}_{init,inner}$ corresponds to a set of desired angular accelerations $\mathrm{d}_{des} \in \mathbb{R}^{\tilde{n}}$ [17]:

$$\dot{x}_{init,inner} = \mathbf{B}_{inner}u \stackrel{!}{=} \mathrm{d}_{des} \tag{4}$$

In general, for $m > \tilde{n}$ the system is over-actuated and there is more than one unique solution to Eq. 4. There are various algorithms and approaches to determine an optimal solution to this equation. An overview of some of the most relevant methods can be found in [17]. One specific method, the pseudo-inverse allocation, is introduced in detail later.

2.2 Control Allocation Problem in Context of Lateral Aircraft Control

Figure 2 displays the roll of the control allocation within the flight control system. It converts desired angular accelerations into physical control surface deflections. The desired angular accelerations themselves are provided by the flight control laws, which, in turn, ensure the tracking of the pilot command u_{pilot}.

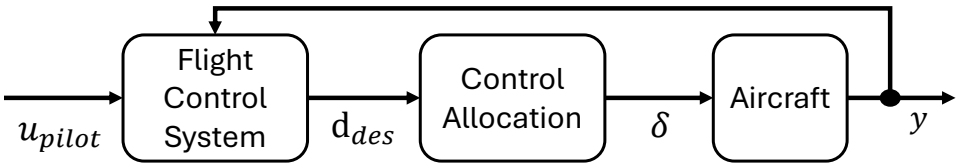

Figure 2 – Block Diagram Displaying the General Concept of Control Allocation

For the specific case of an aircraft's lateral dynamics, the vector $\mathrm{d}_{des,lat}$ consists of the desired roll acceleration $\dot{p}_{des}$ and yaw acceleration $\dot{r}_{des}$:

$$\mathrm{d}_{des,lat} = [\dot{p}_{des}\ \dot{r}_{des}]^T \tag{5}$$

Assuming that the aircraft is equipped with l roll-governing control surfaces at the wing's trailing edge $\delta_{w,i}$, i.e. ailerons and flaps, and one rudder δ_r the corresponding lateral control vector $u_{lat} \in \mathbb{R}^{l+1}$ is:

$$u_{lat} = [\delta_{w,1}\ \delta_{w,2}\ \ldots\ \delta_{w,l}\ \delta_r]^T \tag{6}$$

Consequently, the relevant control sub-matrix is $\mathbf{B}_{inner,lat} \in \mathbb{R}^{2\times(l+1)}$.

2.3 Pseudo-Inverse Control Allocation

In general, Eq. 4 represents an underdetermined linear system of equations with the rank of the matrix $\mathbf{B}$ being equal to the number of elements in d_{des}. In this case Eq. 4 can be solved using $\mathbf{B}_{inner}^{\#} \in \mathbb{R}^{m \times \tilde{n}}$, a pseudo-inverse of matrix $\mathbf{B}_{inner}$. According to the definition used in [17] a pseudo-inverse is a non-square matrix that results the identity matrix when being right-multiplied:

$$\mathbf{B}_{inner}\mathbf{B}_{inner}^{\#} = \mathbf{I}_m \tag{7}$$

Using pseudo-inverse control allocation, the control vector u is allocated by:

$$u = \mathbf{B}_{inner}^{\#}\mathrm{d}_{des} \tag{8}$$

Given the definition of $\mathbf{B}_{inner}^{\#}$, stated in Eq. 7 it can be shown that Eq. 8 provides a solution to Eq. 4:

$$\dot{x}_{init,inner} = \mathbf{B}_{inner}u = \mathbf{B}_{inner}\mathbf{B}_{inner}^{\#}\mathrm{d}_{des} = \mathrm{d}_{des} \tag{9}$$

For $\tilde{n} < m$ there is more than one matrix that meets the pseudo-inverse requirement stated in Eq. 7, allowing for additional design criteria. In [17] this secondary requirement is given by the minimization of the performance index J:

$$\min_u J = \min_u \frac{1}{2} u^T \mathbf{W} u \tag{10}$$

with $\mathbf{W} \in \mathbb{R}^{m \times m}$ being the weighing matrix for the elements of the control vector u. As shown in [17] the pseudo-inverse solving this secondary requirement is given by:

$$\mathbf{B}_{inner}^{\#} = \mathbf{W}^{-1}\mathbf{B}_{inner}^{T}\left(\mathbf{B}_{inner}\mathbf{W}^{-1}\mathbf{B}_{inner}^{T}\right)^{-1} \tag{11}$$

The secondary objective given in Eq. 10 is not connected to the system's states or outputs. Therefore there is no linkage to the performance level of the controlled system. Instead, it is the designer's responsibility to adjust the coefficients of the matrix $\mathbf{W}$ to accomplish certain requirements regarding the system's response. This can either be done by hand or with another optimization problem. As the closed-loop performance is also dependent on the higher level flight control laws, it can be necessary to simultaneously optimize control allocation and flight control laws leading to undesirable, large-order optimization problems.

3. Extended Inverse Control Allocation for Flexible Aircraft

The concept of pseudo-inverse control allocation is based on the fact that there are more effective inputs than elements in the desired accelerations vector d_{des}. Instead of calculating a pseudo-inverse object to a secondary requirement regarding the weighing of the elements of the control vector u as shown in the previous section, this paper is approaching the problem by imposing secondary requirements already in the definition of the control allocation problem stated in Eq. 4. In the following sub-sections the general concept is introduced first. Afterwards, it is shown how this method can be applied to the lateral control allocation of flexible aircraft.

3.1 General Concept of the Extended Inverse Control Allocation

The idea of ECA is to increase the number of states considered in the allocation problem such that it matches the number of available control inputs. This is done by extending the inner derivative vector with elements of the remaining state derivative vector $\dot{x}_{remain}$ such that the dimension of the inner derivative vector is equal to the number of effective control inputs, i.e. $\dot{\tilde{x}}_{inner} \in \mathbb{R}^m$. The corresponding elements in the extended desired accelerations vector $\tilde{\mathrm{d}}_{des}$ are set to zero.

$$\dot{\tilde{x}}_{inner} = \begin{bmatrix} \dot{x}_{inner} \\ \dot{\tilde{x}}_{remain} \end{bmatrix} \text{with } \dot{\tilde{x}}_{remain} \in \mathbb{R}^{(m-\tilde{n})} \subset \dot{x}_{remain} \tag{12}$$

$$\tilde{\mathrm{d}}_{des} = \begin{bmatrix} \mathrm{d}_{des} \\ 0 \end{bmatrix} \tag{13}$$

This way, the relevant control sub-matrix $\tilde{\mathbf{B}}_{inner}$ becomes squared. As long as this matrix consists of linearly independent lines, there is now a proper inverse matrix $\tilde{\mathbf{B}}_{inner}^{-1} \in \mathbb{R}^{m \times m}$ to it. Similar to Eq. 10, the allocation of the control vector u is given by:

$$u = \tilde{\mathbf{B}}_{inner}^{-1} \tilde{\mathrm{d}}_{des} \tag{14}$$

$$\dot{\tilde{x}}_{init,inner} = \tilde{\mathbf{B}}_{inner} u = \tilde{\mathbf{B}}_{inner} \tilde{\mathbf{B}}_{inner}^{-1} \tilde{\mathrm{d}}_{des} = \tilde{\mathrm{d}}_{des} \tag{15}$$

The physical interpretation of this method is, that each state added to the control allocation problem and its respective line of the control matrix represent one secondary design requirement resulting in a balanced number of degrees of freedom (control effectors) and requirements. As Eq. 15 indicates, this procedure uncouples all elements of $\dot{\tilde{x}}_{init,inner}$. The resulting allocation of u, therefore, ensures that a desired maneuver acceleration in d_{des} can be established without an initial reaction in any of the states included in $\dot{\tilde{x}}_{remain}$.

3.2 Application to Lateral Control Allocation for Flexible Aircraft

Based on the notation introduced in equations 5 and 6 the basic control allocation problem of the lateral control of an aircraft with a multi-control surface wing has a total of $l+1$ independent control inputs. After accounting for the primary objective of controlling $\dot{p}_{des}$ and $\dot{r}_{des}$, $l-1$ degrees of freedom remain. Therefore, to minimize the interaction between the (lateral) rigid-body dynamics and the aeroelastic characteristics of the aircraft, the inner derivative vector is extended by $l-1$ modal accelerations $\ddot{\eta}_i$, referring to free-free vibration modes of the modal base, resulting in the following squared allocation problem:

$$\tilde{x}_{inner,lat} = [\dot{p}\ \dot{r}\ \ddot{\eta}_1\ \ldots\ \ddot{\eta}_{l-1}]^T \in \mathbb{R}^{(l+1)} \tag{16}$$

$$u_{lat} = [\delta_{w,1}\ \delta_{w,2}\ \ldots\ \delta_{w,l}\ \delta_r]^T \in \mathbb{R}^{(l+1)} \tag{17}$$

$$\tilde{\mathbf{B}}_{inner} = \begin{bmatrix} \text{——} & b_{\dot{p}} & \text{——} \\ \text{——} & b_{\dot{r}} & \text{——} \\ \text{——} & b_{\ddot{\eta}_1} & \text{——} \\ & \ldots & \\ \text{——} & b_{\ddot{\eta}_{l-1}} & \text{——} \end{bmatrix} \in \mathbb{R}^{(l+1)\times(l+1)} \tag{18}$$

As the total number of modeled aeroelastic modes is typically larger than the number of remaining degrees of freedom, one must carefully decide, which states to include in the extended desired accelerations vector. In this paper, an eigenvector analysis, shown in the next section, is conducted for the reference aircraft to determine which flexible states show the highest degree of interaction with the lateral rigid-body eigenmotions and are therefore worth to be included in the allocation problem.

4. Reference Aircraft DLR-D2AE

The DLR-D2AE serves as a reference aircraft for numerical testing of the modified control allocation. The aircraft, which is displayed in Fig. 3, was developed by the German Aerospace Center (DLR) as a more flexible single-aisle transport aircraft for scientific studies. The design is based on the DLR-D239+, which features similar design characteristics as the Airbus A321 [18]. The most significant modification of the D2AE compared to the D239+ is an elongated wing resulting in a wing aspect ratio of 12.39 [18]. This section briefly introduces the simulation environment modeling the aircraft dynamics and discusses the roll control characteristics. Moreover, the aircraft dynamics are analyzed to identify the relevant flexible modes for the extended inverse control allocation algorithm. In addition, the structure of the lateral flight control law, implemented for this reference aircraft, is presented.

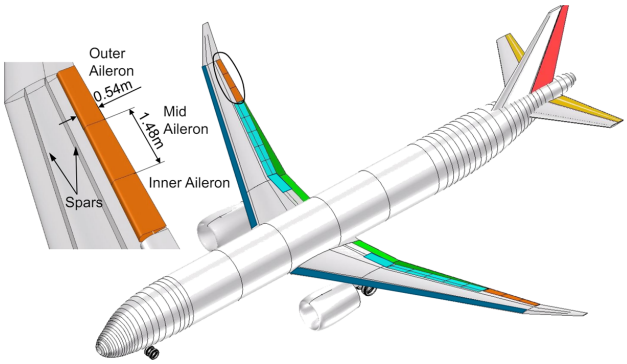

Figure 3 – Rendering of the Reference Aircraft DLR-D2AE [18]

4.1 Simulation Environment

The flight dynamics model used herein employs the methodology developed by Silvestre and Paglione for modeling of moderate flexible aircraft [3], based on the equations of motion proposed by Waszak, Buttrill and Schmidt [19]. To this end, the aircraft dynamics are written based on the linearized mean axes constraints, i.e., the inertial couplings between rigid-body and elastic degrees of freedom are neglected. The structural dynamics are linearly represented in terms of the in-vacuum orthogonal elastic modes of the vehicle. The principle of superposition is applied, resulting in a set of linear second-order differential equations in the modal coordinates η. An unsteady strip theory formulation in the time-domain is used to determine the incremental aerodynamics - due to elastic deformations [20]. The induced forces and moments are calculated utilizing exponential approximations of the Wagner function as proposed in [21]. The final system x_{total} is therefore compounded of the rigid-body dynamics of motion x_{RB}, including the incremental aerodynamics induced by the aircraft flexibility, along with the structural dynamics η and a set of aerodynamic lag states λ:

$$x_{total} = \left[u\ v\ w\ p\ q\ r\ \Phi\ \Theta\ \Psi\ x_e\ y_e\ H\ \eta^T\ \dot{\eta}^T\ \lambda^T\right]^T \tag{19}$$

with the body-frame velocities u, v, and w, the angular velocities p, q, and r, the Euler angles Φ, Θ, and Ψ, the position coordinates x_e and y_e as well as the altitude H. The present simulation architecture, developed in Matlab/Simulink , is given in more details in Fig. 4.

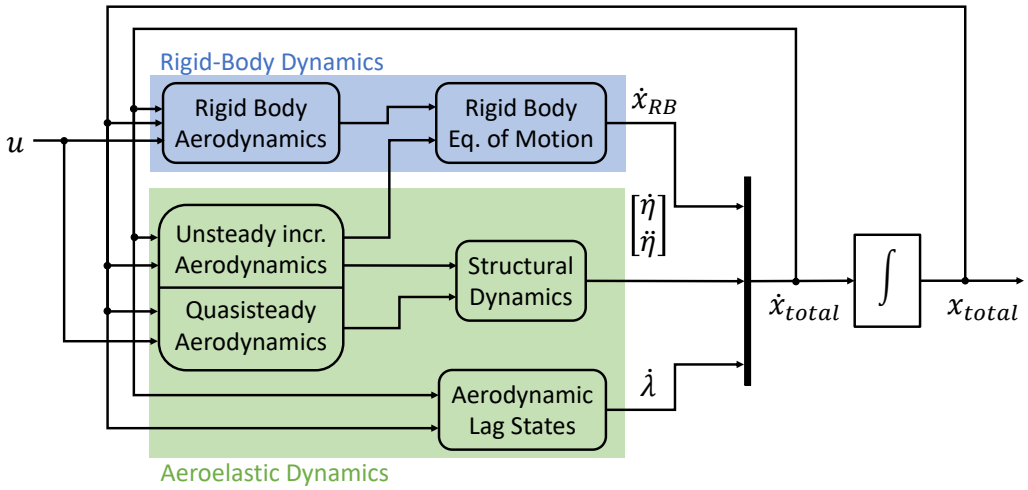

Figure 4 – Block Diagram of the Flexible Dynamics Simulation Model

In short, based on the aircraft state and elastic dynamics, the spanwise downwash and the acceleration associated therewith are determined. The strip-wise aerodynamic lag acceleration is then calculated and input into the unsteady incremental aerodynamics calculation. Moreover, the rigid-body aircraft states and control inputs determine the aeroelastic dynamics while the aeroelastic dynamics provide the incremental aerodynamic forces and moments due to the elastic deformations.

4.2 Roll Control Characteristics

As Fig. 3 shows, the D2AE is equipped with two flaps per wing and three aileron pairs. Each aileron pair is conventionally linked but independent from the other two aileron pairs, resulting in three independent control variables inner aileron $\delta_{a,i}$, mid aileron $\delta_{a,m}$, and outer aileron $\delta_{a,o}$. For the purpose of this paper, it is assumed that the flaps can also be deflected independently from each other and in both directions, making them suitable for roll control. Similar to the ailerons, both inner as well as outer flaps are paired to minimize the influence on the longitudinal dynamics. This results in two additional control variables: $\delta_{f,i}$ for the inner flap pair and $\delta_{f,o}$ for the outer flap pair. Together with the rudder δ_r, the aircraft's lateral control vector therefore consists of six independent elements:

$$u_{lat} = [\delta_{a,i}\ \delta_{a,m}\ \delta_{a,o}\ \delta_{f,i}\ \delta_{f,o}\ \delta_r]^T \tag{20}$$

Thus, four design degrees of freedom remain, allowing to extend the allocation problem by including four modal accelerations $\ddot{\eta}_i$. The mode selection is discussed in the following section.

4.3 Structural Dynamics Analysis

As a first step, the characteristics of the flexible eigenmodes are analyzed. An overview of the shapes and the corresponding in-vacuum structural frequencies of each mode is given in Tab. 1. To evaluate the influence of each mode on the rigid-body dynamics of the reference aircraft, an eigenvector analysis is conducted. Figure 5 displays the resulting normalized eigenvector for all rigid-body modes.

No.	Shape	ω_i [rad/s]
1	sym. bending	12.37
2	asym. bending	16.74
3	asym. bending	21.93
4	fuselage + sym. bending	23.93
5	sym. bending	26.29
6	asym. bending	26.67
7	fuselage + sym. bending	30.21
8	sym. bending	30.33
9	asym. bending	31.08
10	sym. bending	32.19
11	asym. bending	32.89
12	asym. bending	41.84

Table 1 – Overview on the Modal Characteristics of the Reference Aircraft

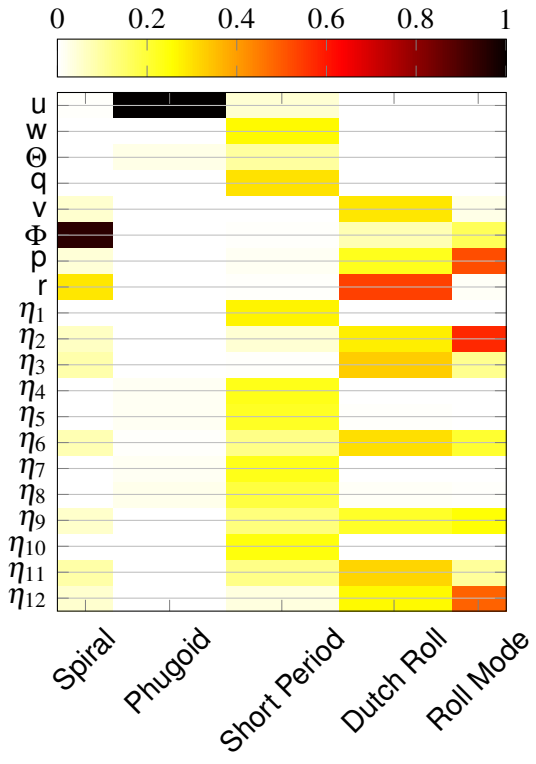

Figure 5 – Contribution of each State to the Rigid-Body Eigenmodes

The eigenvector distribution is determined by linearizing the flight dynamics for a specific flight point, in this case a cruise condition in 7000 m at Mach 0.82. The resulting system matrix is then normalized by dividing each row by the maximum response of the corresponding state to various control inputs. As expected, the lateral eigenmodes (spiral, dutch roll & roll mode) are influenced by the asymmetric bending modes 2, 3, 6, 9, 11, and 12. In the following Fig. 6, the shapes of modes 2 and 12 are displayed, as these are the modes that contribute the most to the roll mode. It can be observed that both modes are dominated by an asymmetric wing bending as indicated in Tab. 1. They are distinguished by the bending order as mode 12 is of higher order with more nodes.

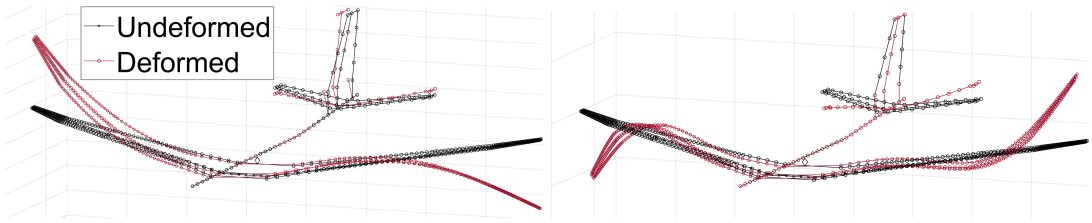

Figure 6 – Modal Shape of Flexible Mode 2 (left) and 12 (right)

Based on the analysis of the structural dynamics, presented in table 1, and its influence on the rigid-body motion, displayed in Fig. 5, two sets of flexible modes to be included in the extended inverse control allocation are considered. The first is to choose those four flexible states that show the highest degree of interaction with the roll mode. Based on Fig. 5 that would result in selecting modes 2, 6, 9, and 12. The second approach is to pick the four asymmetric bending modes with the lowest structural frequency, as increasing frequency separation is expected to decrease the influence on the rigid-body dynamics. This corresponds to modes 2, 3, 6, and 9. This results in the following two candidates for the inner derivative vector of the extended inverse control allocation. Section 5.1 is providing a further discussion on the selection of flexible states to be considered.

$$\tilde{x}_{inner,lat,opt1} = [\dot{p}\ \dot{r}\ \ddot{\eta}_2\ \ddot{\eta}_6\ \ddot{\eta}_9\ \ddot{\eta}_{12}]^T \tag{21}$$

$$\tilde{x}_{inner,lat,opt2} = [\dot{p}\ \dot{r}\ \ddot{\eta}_2\ \ddot{\eta}_3\ \ddot{\eta}_6\ \ddot{\eta}_9]^T \tag{22}$$

4.4 Flight Control Laws

This section provides an overview of the control architecture specifically used for the D2AE to incorporate the flap-integrated control into the flight control system. As indicated by the top-level block diagram of the lateral flight control law in Fig. 2, the control allocation is not directly controlled by the pilot but linked to the base control function, which receives direct inputs from the flight crew.

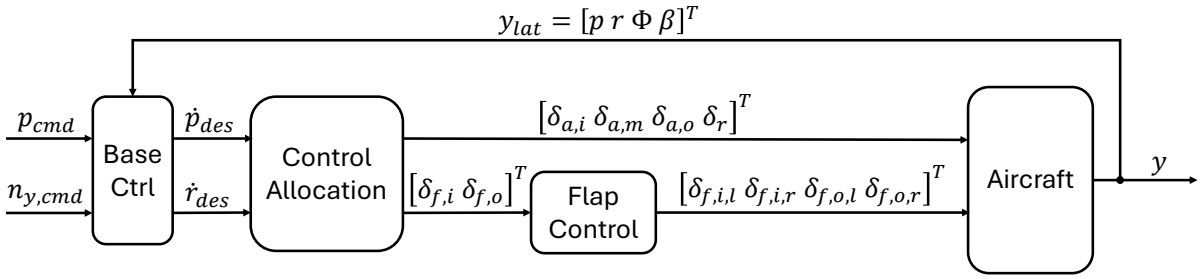

Figure 7 – Block Diagram of the Top-Level Lateral Flight Control Laws

The output of the control allocation, designed as described in section 3.2, are the deflections of the three aileron pairs, the rudder and the two flap pairs. In accordance with the conventional definition of a positive aileron deflection, the flap inputs are defined such that a positive command corresponds to a downward, in the sense of the front-right-down-frame positive, deflection on the right half-wing. In turn, the physical flap deflections are calculated by the flap control block as follows:

$$\delta_{f,i,r} = \delta_{f,i} \qquad \delta_{f,i,l} = -\delta_{f,i}$$

$$\delta_{f,o,r} = \delta_{f,o} \qquad \delta_{f,o,l} = -\delta_{f,o}$$

The second component of the lateral flight control laws is the actual base controller. Based on the pilot-commanded roll rate p_{cmd} and lateral load factor $n_{y,cmnd}$ it determines the elements of d_{des}. In this specific case, the base controller is designed as a multi-input-multi-output feedback tracker:

$$\mathrm{d}_{des} = \mathbf{L}\begin{bmatrix} p_{cmd} \\ n_{y,cmnd} \end{bmatrix} - \mathbf{K}_{y,lat} y_{lat} \tag{23}$$

The feedback matrix $\mathbf{K}_{y,lat} \in \mathbb{R}^{2\times4}$ is determined by eigenstructure-assignment. The objectives are to uncouple the roll and yaw dynamics and to place the poles in position desired according to MIL-STD-1797A [22]. This design is conducted based on the rigid-body lateral state space representation of the aircraft's dynamics. The pre-filter matrix $\mathbf{L} \in \mathbb{R}^{2\times2}$ is determined numerically such that the steady state tracking error for both reference variables is zero.

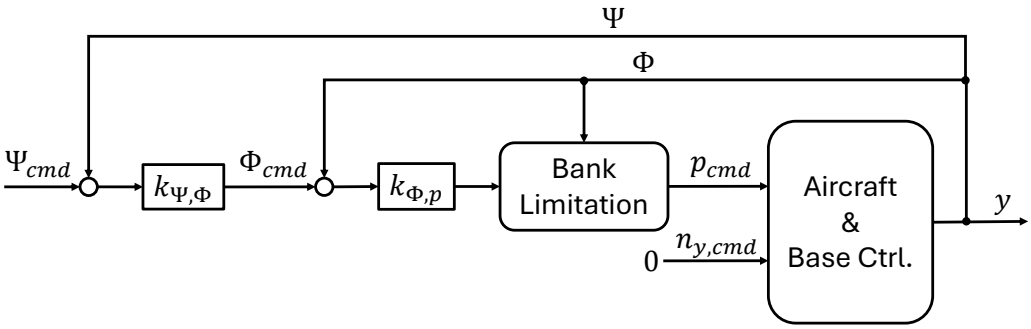

Figure 8 – Block Diagram of the Top-Level Lateral Flight Control Laws

A heading-tracking flight control function is also designed to evaluate the influence of the control allocation on the performance of an auto flight system. As seen in Fig. 8, it extends the base control structure shown in Fig. 7 by a bank angle limitation and a cascaded feedback structure allowing to track a giving heading angle Ψ_{cmd}. The bank angle limitation is realized by a voter concept. The principle of a voting limitation is further discussed in [23], where it is used for a longitudinal flight envelope protection. The gains of the outer cascades are manually tuned such that the tracking performance satisfies the requirements given by MIL-DTL-9490E [24].

5. Evaluation of Flap-Integrated Roll Control Law

To evaluate the influence of the proposed ECA, a comparison with two other control allocation methods is presented in this section for a cruise flight case with an altitude of 7000 m at Mach 0.82 in standard atmosphere. The first configuration considered in this comparison serves as a baseline using only the ailerons (referred to as AO for "ailerons only"). In this case, all three ailerons are deflected symmetrically, artificially creating one large aileron. The second reference configuration is designed with the conventional **p**seudo-**i**nverse **c**ontrol **a**llocation (short PICA) according to [17] as presented in section 2.3. The weighing matrix $\mathbf{W}$ is adjusted manually under the constraint that both flaps are weighted equally as well as all three ailerons being weighted equally.

$$\mathbf{W} = \mathtt{diag}\left(\begin{bmatrix} w_a & w_a & w_a & w_f & w_f & w_r \end{bmatrix}^T\right) \tag{24}$$

As expected based on the findings of [11], is it favorable for the roll performance to weigh the flaps less, i.e. to prefer flap over aileron deflection, in cruise (high-speed) conditions. A parameter study showed that $w_a \geq 3w_f$ is reasonable for the specific test case. The weighting coefficient of the rudder had a negligible influence on the solution of the control allocation problem. This is because the primary objective of the allocation problem, stated in Eq. 5, is to uncouple the roll and yaw acceleration. As the rudder is the only control surface that primarily controls the yaw motion, its deflection is mostly driven by fulfilling the primary allocation requirement. Thus, the influence of its weighing factor w_r on the allocation solution is low. For simplicity, the rudder weighting factor was set equal to the one of the flap $w_r = w_f$, resulting in the following weighting matrix:

$$\mathbf{W} = \mathtt{diag}\left(\begin{bmatrix} 3 & 3 & 3 & 1 & 1 & 1 \end{bmatrix}^T\right) \tag{25}$$

In this section, the application of the new algorithm on the reference aircraft is discussed first. Second, the influence on the roll-performance of the base controller is evaluated. Lastly, the allocation algorithms are compared regarding their performance in a closed loop heading tracking.

5.1 Application of new Control Allocation Algorithm on Reference Aircraft

In section 4. two options of which flexible states to consider for the ECA are proposed in Eq. 21 and 22. Figure 9 compares the closed loop roll-performance of both options based on the system response to a $p_{cmd} = 5°/s$ step input.

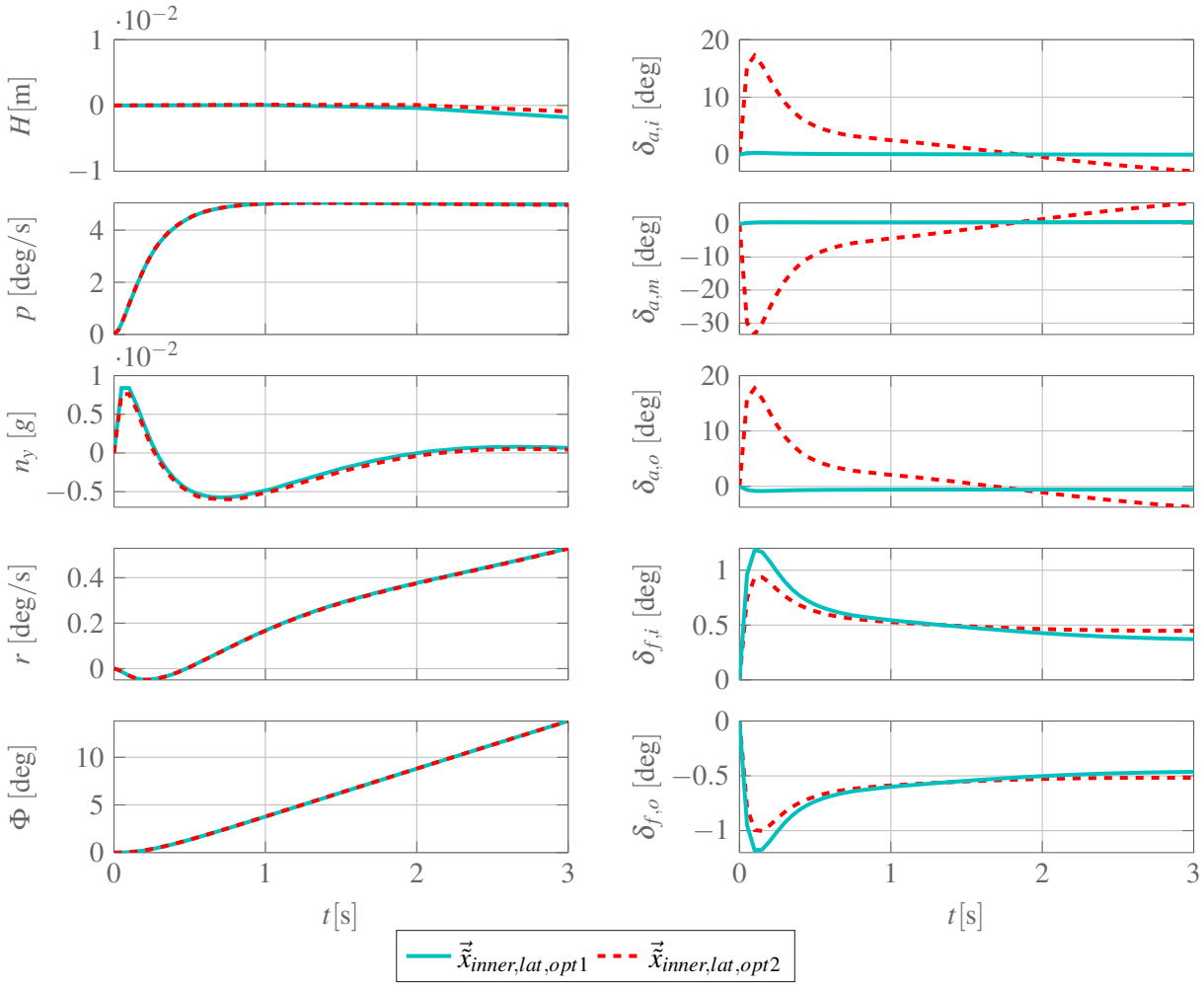

Figure 9 – Comparison of Roll Rate Step Responses for two Different Sets of Flexible Modes Considered for the Extended Inverse Control Allocation Problem

The system's output are highly alike with both extensions of the control allocation problem. Yet, option 2, that considers the modal states 2, 3, 6, and 9 results in a significantly higher aileron deflections. As this is generally undesirable, option 1, considering modal states 2, 6, 9, and 12 is preferred. The step response of option 1 visualizes one interesting characteristic of the ECA. The five control surfaces on the wing are not all deflected in the same direction. While the outer aileron $\delta_{a,o}$ and outer flap $\delta_{f,o}$ are deflected negatively as required for a positive roll rate, the others are deflected in the opposite direction, seemingly counteracting the desired motion. Figure 10 provides an impression of orientation and relative deflection magnitude of the lateral control surfaces.

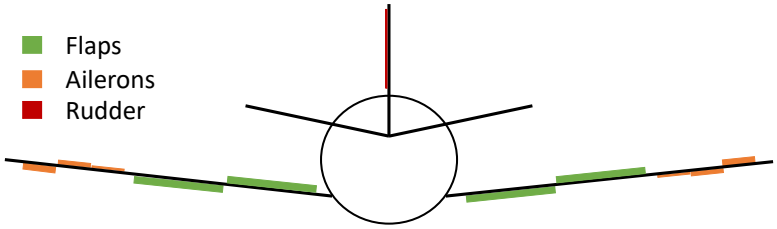

Figure 10 – Qualitative Display of Control Surface Deflections during Roll Command according selected Extended Inverse Control Allocation

This counteracting deflection is a direct consequence of the ECA given by Eq. 15. I.e. it reduces the excitation of the flexible modes, considered in the allocation problem. Still, this allocation leads to overall higher deflections of the control surfaces as fewer control surfaces contribute with a needed positive roll moment and those surfaces must additionally compensate for the counteracting moment of the other control surfaces. When all surfaces are deflected in the same direction, the load can be split between more effectors and there is no counteracting moment to be compensated. In turn, the same roll rate can be accomplished with smaller deflection, when all surfaces deflect in the same direction.

5.2 Comparison of Control Allocation Algorithms based on Roll Performance

Before analyzing the system's response, it is first worth comparing the surface deflections shown in Fig. 11 right. By definition, all three ailerons deflect in the same direction with the same magnitude for the baseline AO-configuration. Similarly, for the PICA configuration, all five surfaces also deflected negatively, as expected for a positive roll command. This is in contrast to the ECA, which, as shown in the previous section, has counteracting deflections. It is due to the definition of the performance index, given by Eq. 10, that the conventional PICA inevitably causes a uniform deflection direction. The performance index used for the PICA weighs the control inputs only. I.e., it favors allocation settings with small deflections. As explained in the previous section, counteracting deflections come with generally larger overall deflections. Therefore an allocation with opposing control inputs cannot be a minimizing solution of the performance index in Eq. 10 and is thereby not attainable with the PICA algorithm.

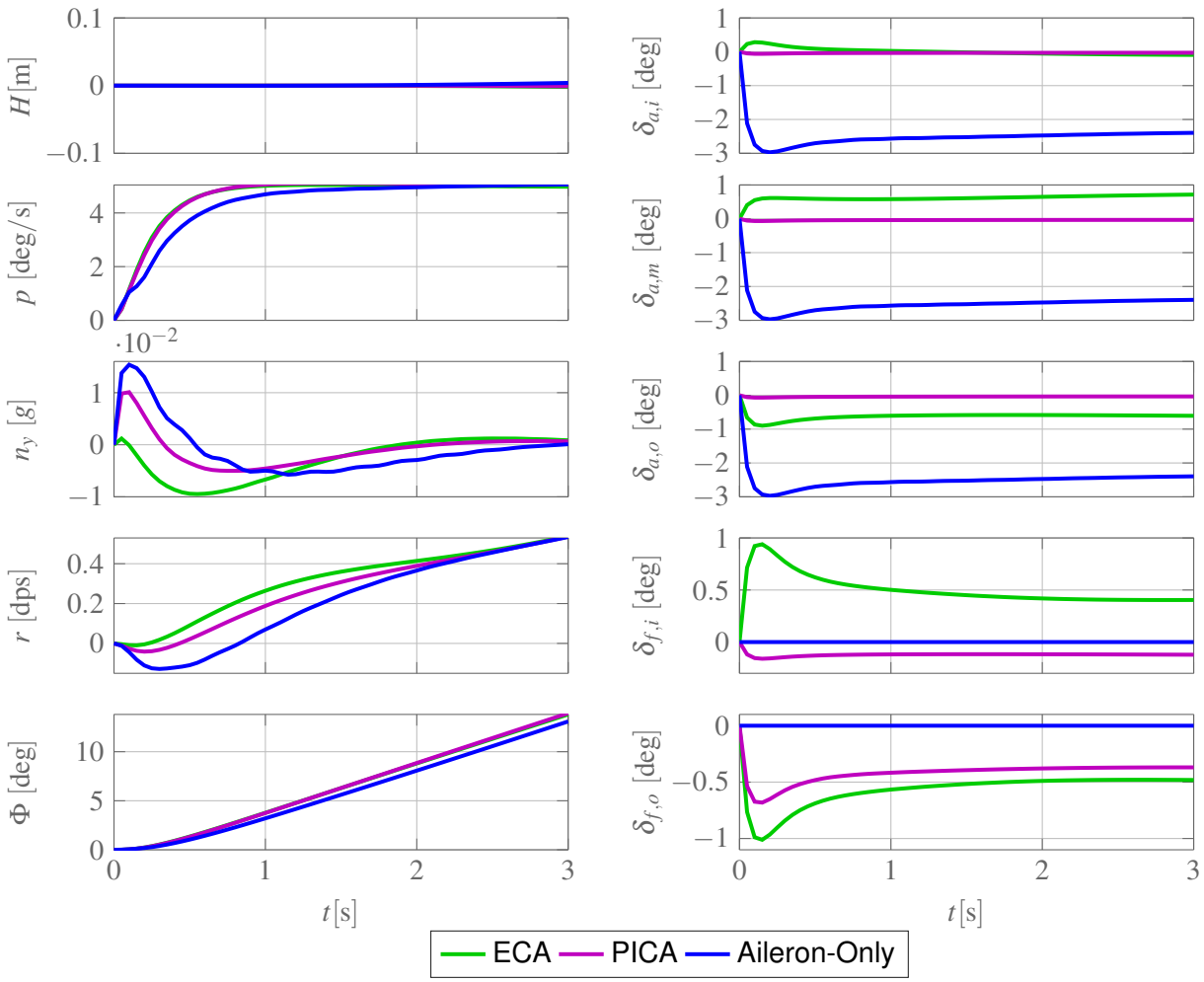

Figure 11 – Comparison of Roll Rate Step Responses for three Different Control Allocation Approaches

When analyzing the time response with the three different allocation approaches, the aileron-only

configuration deviates significantly from the other two. First of all, there is a much more pronounced adverse yaw effect, most obvious in the yaw rate r, which also negatively influences the roll rate p. In addition, the lateral load factor indicates a superposition with a high-frequency oscillation. This is most likely caused by a stronger coupling to the flexible dynamics of the aircraft. The system responses of the other two configurations are barely distinguishable regarding the roll rate response. Yet, the ECA results in a smaller adverse yaw effect than the PICA, as the yaw rate r indicates.

5.3 Comparison of Control Allocation Algorithms based on Heading Tracking Performance

The heading tracking flight control function, presented in Fig. 8, is tested with all three control allocation algorithms simulating the response of a linear model to a reference step input of $\Delta\Psi = 15$ deg. This models a common maneuver a flight crew may command when being vectored by air traffic control, e.g. during approach. The systems' responses are depicted in Fig. 12.

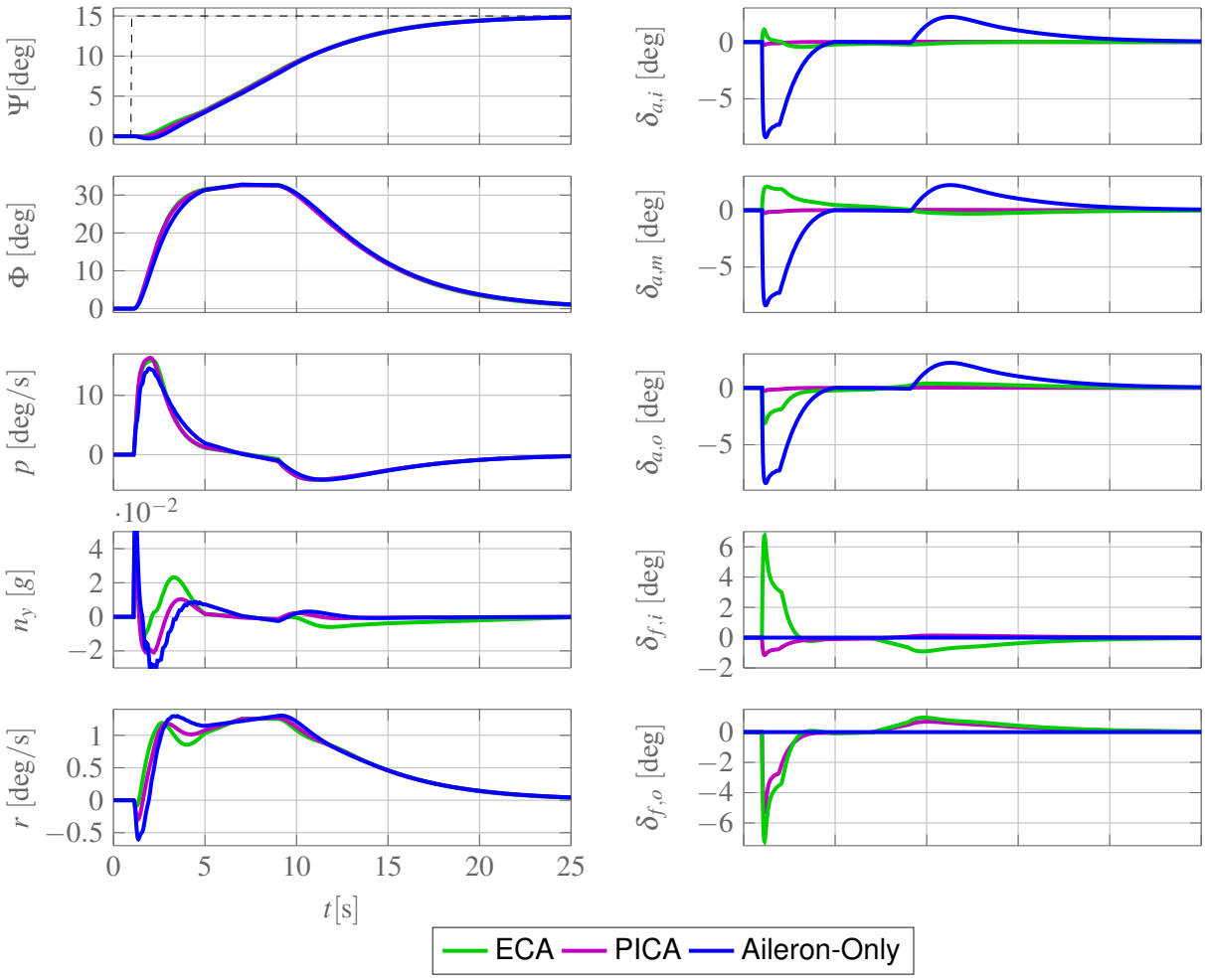

Figure 12 – Comparison of Heading Tracking Performance for three Different Control Allocation Approaches

When analyzing the system outputs, there are only marginal differences between the three approaches. Similar to the findings in the previous section, one can again observe a superposing, high-frequency oscilation in the lateral load factor with the aileron-only configuration, which indicates a higher interaction with the flexible dynamics. In addition, the differences in the adverse yaw effect during turn initiation are present again, with the ECA having the smallest contribution in this regard. Yet, the influence of the more pronounced adverse yaw effect of the other two configurations on the overall performance is negligible, as the time offset in the tracking of Ψ is below 0.1 s. In addition to the time response, the frequency response of the closed-loop systems is also analyzed. The corresponding Nyquist diagrams are displayed in Fig. 13.

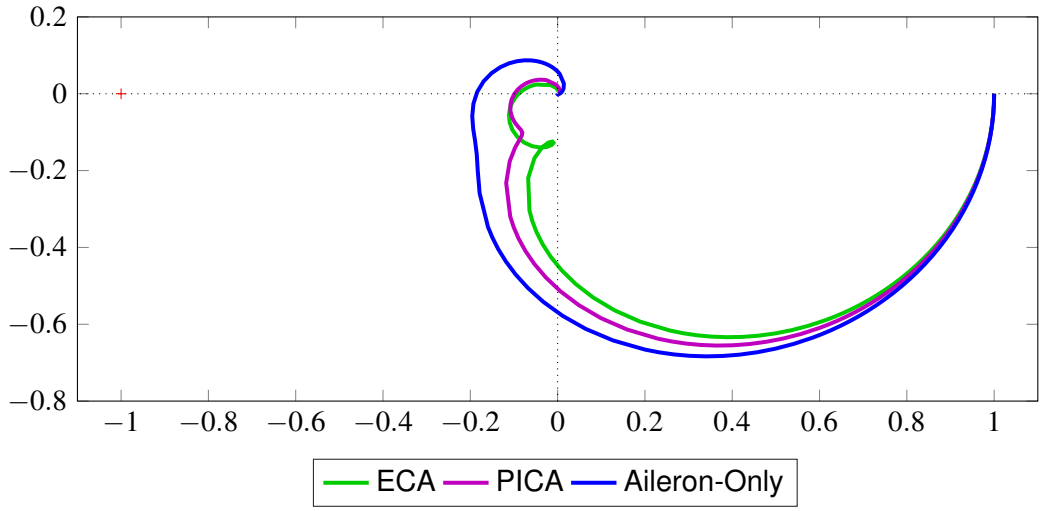

Figure 13 – Closed-Loop Nyquist Diagram for the three Different Control Allocation Approaches

The following Tab. 2 provides an overview on the stability margins of the closed loop system with different the three different allocation concepts. As the Nyquist diagrams indicate, the gain margin of the aileron-only configuration is significantly lower. The difference between the other two configurations is marginal, with the ECA having a slightly better gain margin.

	Aileron-only	**PICA**	**ECA**
Gain Margin [dB]	14,6	20,1	21,0
Phase Margin [deg]	180	180	180

Table 2 – Stability Margins of the Closed-Loop Heading Tracker for the three Differen Control Allocation Approaches

6. Conclusion

Differently to traditional aircraft concepts, modern airliners are equipped with multiple, redundant control surfaces resulting in over-actuated systems with additional degrees of freedom for design process of flight control systems. In this paper the the use of flaps as addition roll control surfaces in the context of multi-functional control devices is investigated. The main objective of this approach is to minimize the influence of the flexible dynamics on the rigid-body performance. For this purpose, a new control allocation approach, the extended inverse control allocation, is introduced, which already accounts for the flexible dynamics in the allocation problem itself. It is then implemented on a more flexible, single-aisle, mid-range transport aircraft. To evaluate the performance, a simulation-based comparison with an aileron-only control allocation and another flap-integrated approach, designed by pseudo-inverse control allocation, is conducted. Based on the findings of this study, two conclusions can be made. First, it is shown, that for a more flexible aircraft, it is generally advantageous to utilize the flaps for roll control in cruise. Second, the newly introduced control allocation method proved to be slightly superior in regard of roll performance compared to the conventional pseudo-inverse control allocation, mostly because the adverse yaw effect is better suppressed and the closed-loop gain margin can be further improved.

7. Acknowledgement

This study was financed in part by the German Federal Ministry for Economic Affairs and Climate Action (BMWK) due to a resolution of the German Federal Parliament within the scope of the LuFo VI-2 project WISDOM (Grant number 20Y2105E).

Copyright Statement

References

[1] Jakub Skoczylas, Sylwester Samborski, and Mariusz Kłonica. The application of composite materials in the aerospace industry. *Journal of Technology and Exploitation in Mechanical Engineering*, 5(1):1–6, 01 2019.

[2] J.R.R.A. Martins, G. Kennedy, and G.K. Kenway. High aspect ratio wing design: Optimal aerostructural tradeoffs for the next generation of materials. *AIAA SciTech*, 01 2014.

[3] F.J. Silvestre and P. Paglione. Dynamics and control of a flexible aircraft. *AIAA Atmospheric Flight Mechanics Conference and Exhibit*, August 2008.

[4] C.M. Shearer and C.E.S. Cesnik. Trajectory control for very flexible aircraft. *Journal of Guidance, Control, and Dynamics*, 31(2), March 2008.

[5] R.L. Bisplinghoff, H. Ashley, and R.L. Halfman. *Aeroelasticity*. Dover Publications, 1996.

[6] F.J. Silvestre et al. Aircraft control based on flexible aircraft dynamics. *Journal of Aircraft*, 44(1), January 2017.

[7] S. Düssler, T. Mylvaganam, and R. Palacios. Lqg-based gust load alleviation systems for very flexible aircraft. *AIAA SciTech Forum 2023*, January 2023.

[8] X. Wang et al. Seamless active morphing wing simultaneous gust and maneuver load alleviation. *Journal of Guidance, Control, and Dynamics*, 44(9):1649 – 1662, May 2021.

[9] N. Fezans, H.D. Joos, and Deiler C. Gust load alleviation for a long-range aircraft with and without anticipation. *CEAS Aeronautical Journal*, 10, 01 2019.

[10] S. Delannoy. A380 roll kinematics design. *IFAC Proceesings*, 40(7), 2007.

[11] D. Sanghi et al. Influence of aileron placement on roll response of high-aspect-ratio-wing aircraft. *2020 AIAA AVIATION Forum*, June 2006.

[12] B.N. Nield. An overview of the boeing 777 high lift aerodynamic design. *The Aeronautical Journal*, 99(989), November 1996.

[13] V. Manvi. Beware!!! clear air turbulence - united boeing 777 300er. https://www.youtube.com/watch?v=7-JwqNe-Mag, November 2018.

[14] K. Ning and S. YouMin. Variable camber differential flap technology applied in aircraft high lift system. *CSAA/IET International Conference on Aircraft Utility Systems*, June 2018.

[15] T. Lampl and M. Hornung. An integrated design approach for advanced flight control systems with multi-functional flight control devices. *AIAA AVIATION Forum*, June 2018.

[16] P. Eichhorn and F.J. Silvestre. Evaluation of an automatic continuous high-lift system in a flight simulator study with airline pilots. *CAES Aeronautical Journal*, 15(2), December 2023.

[17] M.W. Oppenheimer, D.B. Doman, and M.A. Bolender. Control allocation for over-actuated systems. 14^{th} *Mediterranean Conference on Control and Automation*, June 2006.

[18] T. Klimmek and M. Schulze. Development of a short medium range aircraft configuration for aeroelastic investigations using cpacs-mona. *Deutscher Luft- und Raumfahrtkongress*, September 2022.

[19] Waszak M.R., C.S. Buttrill, and Schmidt D.K. Modeling and model simplification of aeroelastic vehicles: An overview. *National Aeronautics and Space Administration*, September 1992.

[20] F.J. Silvestre and R. Luckner. Experimental validation of a flight simulation model for slightly flexible aircraft. *AIAA Journal*, December 2015.

[21] R.T. Jones. Operational treatment of the nonuniform-lift theory in airplane dynamics. Technical Report MIL-STD-1797A, National Advisory Committee for Aeronautics, Washington DC, United States, October 1938.

[22] United States Airforce (Publ.). Flying qualities of piloted aircraft. Technical Report MIL-STD-1797A, Department of Defence, Washington DC, United States, January 1990.

[23] S. Oudin, S. Delannoy, and P. Debusschere. Low speed protections for a commercial airliner : a practical approach. *AIAA Guidance, Navigation, and Control Conference*, January 2017.

[24] United States Airforce (Publ.). Flight control systems - design, installation and test of piloted aircraft, general specification. Technical Report MIL-DTL-9490E, Department of Defence, Washington DC, United States, April 2008.